Journal of Engineering Science and Technology
Special Issue on WRICET2016, December (2018) 86 - 93

CHARACTERIZATIONS AND BIODEGRADABILITY OF SOLVENT CASTING HALLOYSITE NANOTUBES/SAGO STARCH NANOCOMPOSITE

ZURAIDA AHMAD*, HAZWAN YATIMI HERMAIN,
NUR HUMAIRAH ABDUL RAZAK

Department of Manufacturing & Materials Engineering, Kulliyyah of Engineering,
International Islamic University Malaysia, Gombak, 53100
Kuala Lumpur, Malaysia.
*Corresponding Author: zuraidaa@iium.edu.my

Abstract

The incorporation of nanofiller into bio-based matrixes has gain attention so as to produce a bio-nanocomposite. This approach aids in enhancing the properties of the bio-based matrixes whilst maintaining the environmental friendliness of the nanocomposite. Thus, this paper reports on the characterizations of thermoplastic sago starch (TPSS) which was reinforced with halloysite nanotubes (HNT) to form a bio-nanocomposite. The nanocomposite at varying HNT contents (0, 0.25, 0.5, 1.0, 3.0 and 5.0 wt.%) was fabricated by solvent casting technique. The effect of HNT content on the nanocomposite was studied for its crystallinity, chemical functional groups, thermal analysis and biodegradability. X-ray diffractograms (XRD) revealed higher crystallinity of the nanocomposite as compared to the TPSS. The nanocomposite spectrum, as characterized by Fourier Transform Infrared Spectroscopy (FTIR) showed the presence of Si-O groups of HNT at absorption bands of 1117 cm^{-1}, 1027 cm^{-1} and 1007 cm^{-1}. FTIR also revealed the occurrence of interaction between HNT and starch matrix. Addition of HNT also improved the thermal stability of the nanocomposite with increasing of HNT content. Biodegradability of the nanocomposite, however, reduced at higher HNT content after 60 days of soil burial. Thus, it is concluded that the addition of HNT enhanced the strength of TPSS film and at the same time, easily degraded when dispose into the landfill that make it suitable as biodegradable wound-healing materials.

Keywords: Biodegradability, Casting, Halloysite nanotubes, Nanocomposite, Sago.

1. Introduction

Non-biodegradable petrochemical based plastics have created environmental concerns and so it elevated interest in the use of biopolymers. One of the most promising biopolymers is starch, due to its availability, biodegradability, thermoplastic behavior and relatively low cost [1]. Starch is a renewable natural polysaccharide and can be obtained from a great variety of crop. Unfortunately, starch possesses some weaknesses in terms of mechanical properties, processability, long-term stability and water sensitivity [2]. In order to overcome the problems, starch can be reinforced by fillers, such as nanoparticles, and lead to the development of nanocomposite material [1].

Of late, halloysite nanotubes (HNT) have becoming interesting nanofiller for enhancing thermoplastic polymers' mechanical and thermal properties, fire retardant and crystallinity [1]. HNT, a naturally occurring aluminosilicate, forms a hollow tubular structure. It is a clay mineral with similar structure to kaolinite. Its outer surface has similar properties to that of SiO_2 while the inner cylindrical core is alike Al_2O_3 [1]. The viable nanocage of HNT is applicable for inclusion of biologically active molecules with specific sizes due to the empty space inside the HNT [3]. Moreover, it offers potential application as control release of anti-corrosion agents, fungicides, and herbicides [3, 4]. Additionally, native starch has to be plasticized prior to processing and moulding. Hence, glycerol and water are common plasticizers and mixed with starch before the plastic processing techniques such as extrusion, injection-moulding, compression and solvent casting [1].

Thus, the present study aims to characterize and evaluate TPSS/HNT nanocomposite which was fabricated by solvent casting technique for its chemical and thermal properties as well as biodegradability.

2. Experimental Procedure

2.1. Materials

Sago starch powder was purchased from local retailer, Hup Seng Heng Sdn. Bhd., Malaysia while HNT was supplied by Imerys Tableware Asia Limited, New Zealand. The non-volatile plasticizer, glycerol of 99.5% purity was obtained from Merck Chemicals, Malaysia. Distilled water acted as co-plasticizer.

2.2. Preparation of nanocomposite

Sago starch, glycerol and distilled water at a weight fraction of 6.5:3.5:90, respectively, were stirred and heated until starch gelatinization temperature of 70°C. HNT at varying content of 0, 0.25, 0.5, 1.0, 3.0, and 5.0 wt.% was initially stirred in 15 ml water for 1 hour. The HNT solution was then added to the gelatinized starch and heated to 75-80°C. The solvent was poured and casted on a flat and smooth ceramic tile and dried in the oven for 20 hours at 50°C.

2.3. Testings

The crystallinity of films was characterised by using XRD (SHIMADZU XRD 6000) at 40 kV and 30 mA in the region of 2θ from 5° to 70° with the continuous scan speed of 3°/min.

The chemical group functionalities of HNT and nanocomposite were scanned and evaluated by using FTIR (Spectrum 2000 Perkin Elmer) with 20 scans and 8 cm^{-1}resolution within the range of 500-4000 cm^{-1}.

Thermal analyses of the nanocomposite were examined by using TGA (HITACHI STA7300 Thermal Analysis System) at a temperature range of 40-500°C with the temperature increment rate of 10°C per minute and sampling time of 0.5 seconds. The melting temperature (T_m) and glass transition temperature (T_g) of nanocomposite films were determined by using DSC (Instrument DSC Q20 V24.10 Build 122, INTROP) in an inert atmosphere by flowing nitrogen at the rate of 50ml/min between 30-250°C at a scanning rate of 10°C/min.

Biodegradability of the nanocomposite was determined by measuring the weight loss of the specimens after every 5 days interval in which the specimens were layered in 5-8cm thick compost and incubated for up to 60 days at 25°C.

3. Results and Discussion

3.1. XRD analysis

The X-ray diffractograms of the nanocomposite at 0, 0.25, 0.5, 1, 3, and 5 wt.% HNT are presented in Fig. 1. XRD pattern of control TPSS produced a sharp diffraction peak at 2θ = 9.58° and a broad scattering reflection at around 2θ = 19° indicating that matrix of the pure TPSS has crystalline structure and it its partially amorphous. The incorporation of HNT into the TPSS increases the diffraction peaks of HNT/TPSS nanocomposite at 2θ = 11.89°, corresponding to a basal spacing of 7.44 Å. Similar results were found in HNT/PLA nanocomposite by Liu et al. [5]. The stronger diffraction intensity of HNT/TPSS nanocomposite at the basal reflection of 7.44 Å, as HNT contents increase, implied higher crystallinity of the nanocomposite than TPSS. In addition, other diffraction peaks which show slight increase in intensity can be observed at around 2θ = 19.9°, 2θ = 21.7°, and 2θ = 24.7° which correspond to the basal spacing of 4.43, 4.08, and 3.60 Å, respectively. The increase in peak intensity signifies that the addition of HNT into TPSS increases the crystallinity of the nanocomposite due to the crystalline structure of HNT as reported by Liu et al. [5], where the other two main sharp peaks of HNT were observed at around 20° and 25°. The incorporation of HNT into TPSS matrix therefore reduces the amorphous region and increases the crystallinity of the nanocomposite.

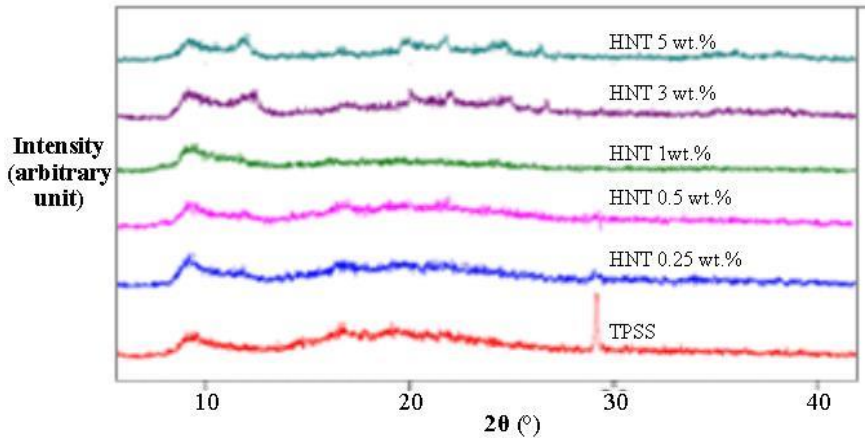

Fig. 1. XRD patterns of HNT/TPSS nanocomposite at varying HNT content.

3.2. FTIR

The FTIR spectra of HNT, TPSS, and nanocomposite at varying HNT contents are shown in Fig. 2. The peak on HNT spectrum detected at 3694 cm^{-1} represents the external hydroxyl groups on the non-shared surface, while the peak at around 3622 cm^{-1} represents the hydroxyl groups located on the aluminium-oxygen octahedron and silicon-oxygen tetrahedron interfaced layer [6]. The HNT spectrum is further characterized by Si-O stretching region, according to Bobos et al. [7], which comprises of three absorption bands at 1117 cm^{-1}, 1027 cm^{-1}, and 1007.71 cm^{-1}. The peaks observed at 909.71 cm^{-1} is due to the Al-OH librations, while the doublet peaks at 533.16 cm^{-1} and 527 cm^{-1} are assigned to the Al-O-Si bending vibrations [7].

The compatibility of the glycerol as the plasticizer in the TPSS was proven by the two stable peaks which represents O-H bond observed at 3269.26 cm^{-1} and 2929.14 cm^{-1} indicating that glycerol could form stable hydrogen bond with sago starch. More characteristic peaks are seen at 1646.26 cm^{-1} and around 1335.05 cm^{-1} which imply C-H bonding. The peak with highest intensity, at 1003.49 cm^{-1}, indicates the C-O bond stretching of C-O-C group. As the amount of HNT added into TPSS increase, the peaks in the range of 3730 cm^{-1} to 3000 cm^{-1} increases in intensity due to the formation of O-H bonding. The characteristic peak at 1003.49 cm^{-1} becomes sharper and slightly shifted to the right at 1001 cm^{-1} due to the existence of Si-O bond attached to HNT. Moreover, some short peaks in range of 560 cm^{-1} to 516 cm^{-1} also increase in intensity, due to the presence of Al-O-Si vibrations obtained from HNT.

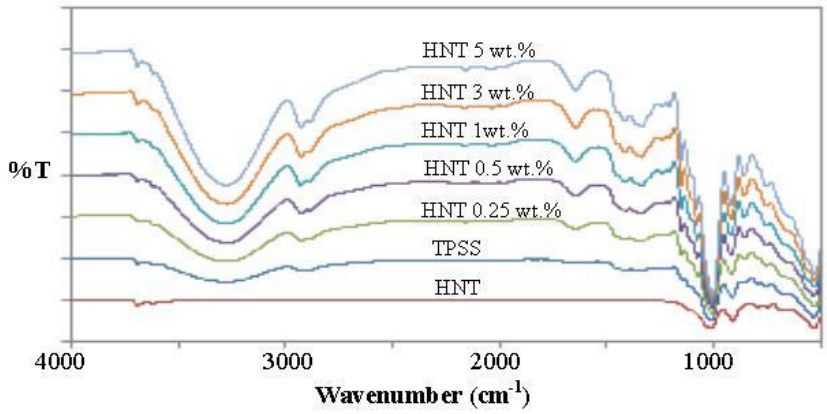

Fig. 2. FTIR spectra of HNT, TPSS, and nanocomposite at different HNT contents

3.3. Thermal analyses

TGA thermograms of the nanocomposite at varying HNT contents are shown in Fig. 3. Three-step degradation of TPSS (0 wt.% HNT) can be observed in this figure, in which the first step at around 100ºC represents the dehydration of the TPSS, the second step from 200°C to around 300°C due to the evaporation of glycerol [8], and the third step in the range of 289.5°C to 334°C mainly caused by degradation of the TPSS itself. The char residue of nanocomposite at temperature above 350°C is significantly increased as the HNT contents are increased.

Results of this study confirm the earlier findings [6, 9]. The increase in thermal stability can be attributed to the effect of HNT particles which constrained the motion of plastic chains, and consequently lead to more char formation [6, 9]. The high barrier properties of nanoparticles are believed to provide a thermal barrier which prevents heat transfer inside polymer matrix. Furthermore, the entrapment of degradation products of TPSS inside the structure of the HNT tubules could lead to the increase in thermal stability as more HNT are included inside the nanocomposite [10].

Figure 4 represents the melting and glass transition behaviours of TPSS and nanocomposite. The DSC thermogram of TPSS exhibited sharp endothermic peak at 195.96 °C (ΔH_m=169.4 J g^{-1}) which have been associated with the melting of crystalline starch domains reorganized during the retrogradation [11]. The melting peak of TPSS/HNT nanocomposite with 0.5 wt% HNT was around 164°C (ΔH_m=199.6 J g^{-1}), which is 31.96°C lower than TPSS (without HNT content). This reduction in T_m and increase in ΔH_m for 0.5 wt% HNT incorporated TPSS was probably attributed to the slightly higher moisture content of 0.5 wt% HNT compared to without HNT. Higher contents of HNT increased the position of the peaks to 188.44°C (ΔH_m=123.2 J g^{-1}) and 204.04°C (ΔH_m=100.3 J g^{-1}) in the nanocomposite containing 3 wt.% and 5 wt.% HNT, respectively.

The change in the position of these peaks indicates that higher HNT content favour the formation of larger crystal domains and lowers the mobility of amylopectin in the starch matrix [11]. The glass transition peaks of nanocomposite at 0.5, 3, and 5 wt.% HNT contents reduce from 156.69 °C to 148.89°C, 151.30°C, and 151.76°C, respectively. The expense of glass transition region for film with 5 wt.% HNT was smaller than that of nanocomposite at lower HNT contents. This is due to well-ordered arrangement and good organization of chains in amorphous region, which in turn increases the degree of crystallinity. Similar trend can be observed in the study of starch-CMC-nanoclay biodegradable films by [11].

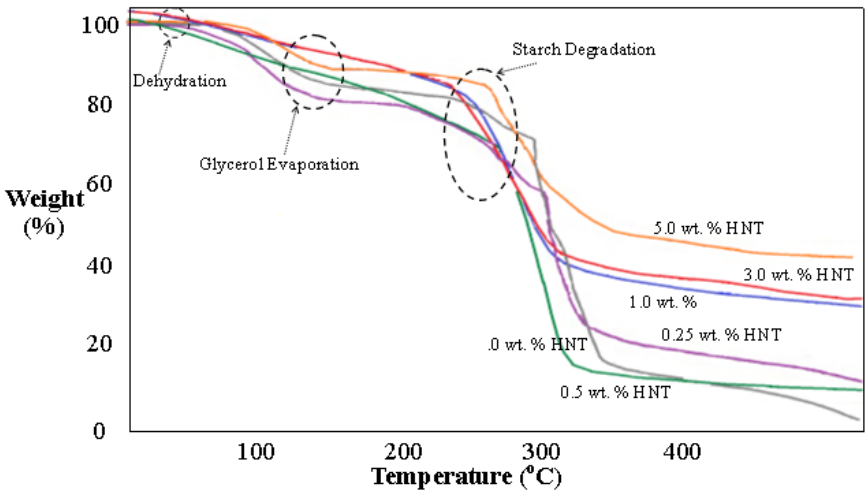

Fig. 3. TGA curves of HNT/TPSS nanocomposite at (a) 0, 0.25, 5.0 wt.% and (b) 0.5, 1.0, 3.0 wt.% of HNT content.

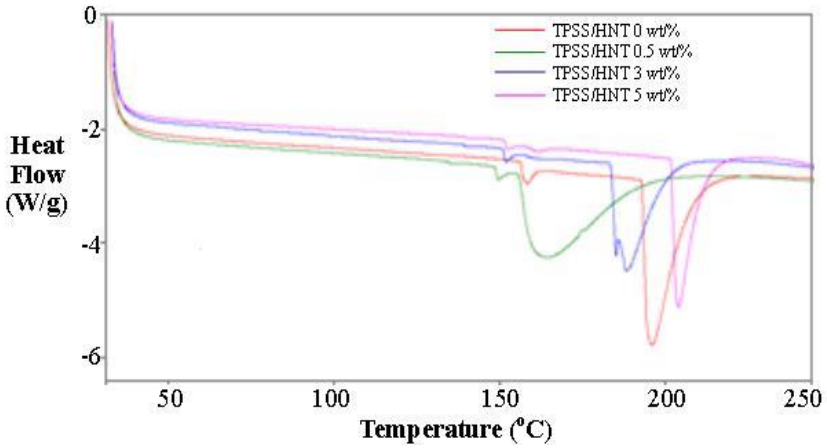

Fig. 4. DSC heating curves of TPSS/HNT nanocomposite.

3.4. Biodegradability

The degradation and weight loss of the nanocomposite at varying HNT loadings are presented in Figs. 5 and 6, respectively. The reaction between TPSS and microorganisms from the compost, such as bacteria, algae, or fungi, begins at the film surface. Once progressed, it results in loss of strength, assimilation by microorganisms, and breakage of backbone chains or degradation by enzymes, and subsequent reduction in the average molecular weight of the nanocomposite.

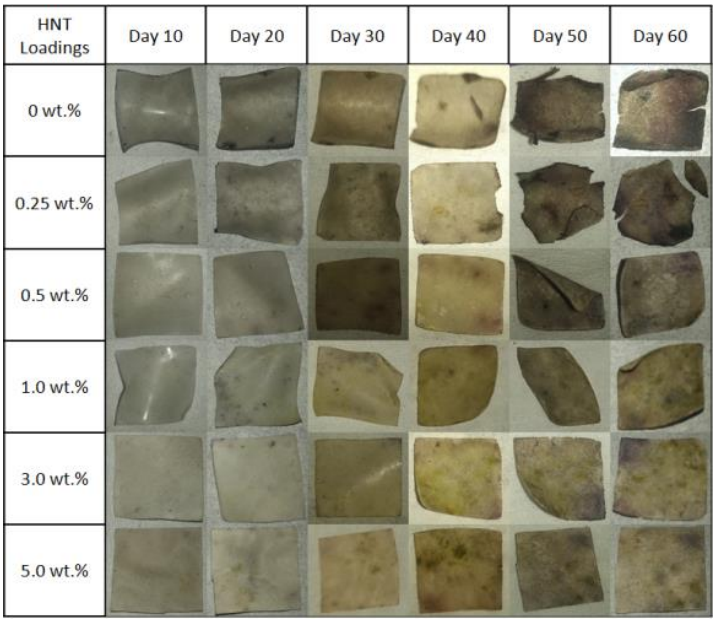

Fig. 5. The degradation condition of the nanocomposites after certain burial days.

Figure 5 shows that composite with 0.25 wt.% HNT content still allowed the formation of cracks, but composite at higher HNT contents did not form any

significant cracks or deformation due to degradation. The cracks will affect the degradation rate since more cracks will expose the surfaces to the action of microbes [12]. In Fig. 6, higher HNT contents result in less weight loss and slower degradation rate. Nevertheless, the nanocomposite still exhibited positive degradation process in 60 days of burial.

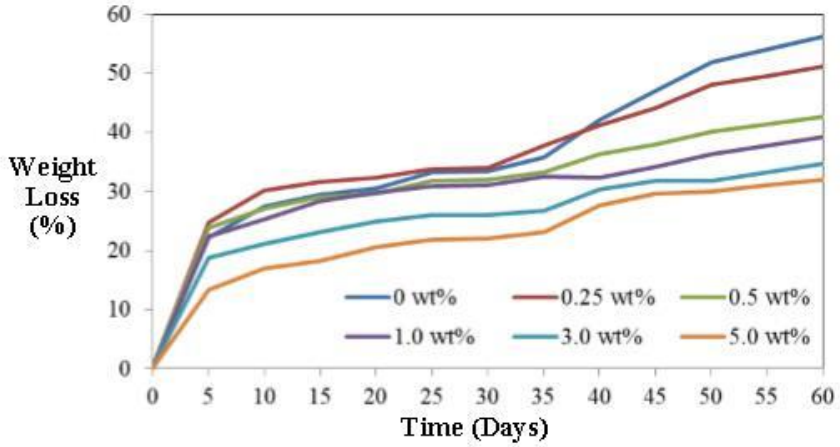

Fig. 6. The weight loss of nanocomposite due to degradation after certain burial days.

4. Conclusions

HNT was introduced into TPSS matrix to produce a bio-nanocomposite, which assisted in increasing crystallinity of nanocomposite. The existence of interaction between HNT and TPSS were proven with the formation of O-H, Si-O, Al-OH, and Al-O-Si bonds, as demonstrated in FTIR analysis. The T_m and T_g of the nanocomposite were reduced at low HNT contents, yet it increased at high HNT contents, which determine the thermal stability enhanced with the addition of HNT. Biodegradability of the nanocomposite, however, was gradually reduced with the increasing of HNT contents but it still degraded at slower pace. It is hoped that the findings from this study offered potential progressive outcomes in the nanomaterial industries.

Acknowledgements

The authors would like to thank International Islamic University Malaysia for the financial support under Research Initiative Grant Scheme (RIGS-17-146-0721).

References

1. Meira, S.M.M.; Zehetmeyer, G.; Scheibel, J.M.; Werner, J.O.; and Brandelli, B. (2016). Starch-halloysite nanocomposites containing nisin: Characterization and inhibition of Listeria monocytogenes in soft cheese. *LWT- Food Science and Technology*, 68, 226-234.
2. Xie, Y.F.; Chang, P.R.; Wang, S.J.; Yu, J.G.; and Ma, X.F. (2011). Preparation and properties of halloysite nanotubes/plasticized Dioscorea opposite Thunb. Starch composites. *Journal of Carbohydrate Polymers*, 83(1), 186-191.

3. Price, R.R.; Gaber, B.P.; and Lvov, Y.M. (2001). In vitro release characteristics of tetracycline HCl, khellin and nicotinamide adenine dineculeotide from halloysite, acylindrical mineral. *Journal of Microencapsulation*, 18(6), 713-722.
4. Shchukin, D.G.; Zheludkevich, M.; Yasakau, K.; Lamaka, S.; Ferreira, M.G.S.; and Mohwald, H. (2006). Layer-by-layer assembled nanocontainers for self-healing corrosion protection. *Advanced Materials*, 18(13), 1672-1678.
5. Liu, M.; Zhang, Y.; and Zhou, C. (2013). Nanocomposites of halloysite and polylactide. *Applied Clay Science*, 75-76, 52-59.
6. Ismail, H.; Khoo, W.S.; and Ariffin, A. (2013). Effect of nanotubes and kaolin loading on tensile, swelling and oxidative degradation properties of poly(vinyl) alcohol/chitosan blends. *Journal of Vinyl and Additive Technology*, 19(1), 55-64.
7. Bobos, I.; Duplay, J.; Rocha, J.; and Gomes, C. (2001). Kaolinite to halloysite - A transformation in the kaolin deposit of Sao Vicente De Pereira, Portugal. *Clays and Clay Minerals*, 49(6), 596-607.
8. Yunos, M.Z.B.; and Rahman, W.A.W.A. (2011). Effect of glycerol on performance rice straw/starch based polymer. *Journal of Applied Sciences*, 11(13), 2456-2459.
9. Soheilmoghaddam, M.; and Wahit, M.U. (2013). Development of regenerated cellulose/halloysite nanotube bionanocomposite films with ionic liquid. *International Journal of Biological Macromolecules*, 58, 133- 139.
10. Alhuthali, A.; and Low, I.M. (2013). Water absorption, mechanical, and thermal properties of halloysite nanotube reinforced vinyl-ester nanocomposites. *Journal of Materials Science*, 48(12), 4260-4273.
11. Almasi, H.; Ghanbarzadeh, B.; and Entezami, A.A. (2010). Physicochemical properties of starch-CMC-nanoclay biodegradable films. *International Journal of Biological Macromolecules*, 46(1), 1-5.
12. Ojijo, V.; and Ray, S.S. (2014). Nano-biocomposites based on synthetic aliphatic polyesters and nanoclay. *Progress in Materials Science*, 62, 1-57.